Dual-Modal Tactile Perception and Exploration

Nicholas Pestell, John Lloyd, Jonathan Rossiter, and Nathan F. Lepora

***Abstract*—Tactile sensing is required for human-like control with robotic manipulators. Multimodality is an essential component for these tactile sensors, for robots to achieve both the perceptual accuracy required for precise control, as well as the robustness to maintain a stable grasp without causing damage to the object or the robot itself. In this study, we present a cheap, 3D-printed, compliant, dual-modal, optical tactile sensor that is capable of both high (temporal) speed sensing, analogous to pain reception in humans and high (spatial) resolution sensing, analogous to the sensing provided by Merkel cell complexes in the human fingertip. We apply three tasks for testing the sensing capabilities in both modes; first, a depth modulation task, requiring the robot to follow a target trajectory using the high-speed mode; second, a high-resolution perception task, where the sensor perceives angle and radial position relative to an object edge; and third, a tactile exploration task, where the robot uses the high-resolution mode to perceive an edge and subsequently follow the object contour. The robot is capable of modulating contact depth using the high-speed mode, high accuracy in the perception task, and accurate control using the high-resolution mode.**

***Index Terms*—Force and tactile sensing, biomimetics.**

I. Introduction

ROBUST and flexible tactile sensing is considered one of the major challenges for future robotics. Where robots are required to physically interact with unknown environments, tactile sensing can help to minimise the risk of damage to the environment and the robot, while enabling the robot to understand the physical nature of its surroundings to interact with the environment in a controlled and intelligent way. For tactile sensors to be useful, they must be highly accurate, small enough for integration with robotic manipulators and be sensitive to a range of tactile features.

This last requirement necessitates multi-modality in future tactile sensors. As the human fingertip is endowed with a range of mechanoreceptors for detecting features such as, texture, hardness and shape [1], tactile sensors must also be equipped with technologies capable of sensing in these distinct modes. There are a handful of tactile sensor with multimodal capabilities [2]–[5], where the emphasis is on sensing high-resolution e.g., point discrimination or force with an additional high-bandwidth sensing for features such as texture. In some cases temperature sensing is also an included modality [6].

We have designed and built a tactile sensor using a small image tracking chip (ADNS-3080 [7]) as an image acquisition system which offers both a high (temporal) speed (single value at $\sim$2000 Hz) and high (spatial) resolution sensing mode (30 $\times$ 30 pixel image, $\sim$3 Hz). The manufacturing cost of this sensor are low ($\sim$£100) and the body is completely 3D-printed, making the manufacturing process relatively simple. We also implement a novel approach to high-resolution sensing based on using raw pixel values as features without the need for any image processing, distinct from past work with 3D-printed optical tactile sensors [8]–[13].

The performance of the presented sensor is tested in a number of tasks. Initially, we verify the performance of the high-speed mode for controlling the sensor contact depth by requiring the sensor to follow a target trajectory whilst maintaining contact with a surface. We then test the performance of the high-resolution mode at perceiving angle and radial distance relative to an edge. Robustness of this perception is then confirmed in a contour following task. Finally, we combine the use of the two modalities into a single task of following the contour of a previously unseen object using the high-speed mode to locate the object depth and edge location (see supplementary video accompanying this paper).

Traditionally, additional modalities have been focused on high-frequency sensing for features such as texture. Similar to the application of a 'reflex mode' in [14], here we instead draw an analogy between high-speed sensing and pain reception. In [14] the sensor is used purely as a force estimator, whereas, in the presented study we use both modalities to perceive multiple dimensions (angle, radial position and depth) and use the perceived state to control the motion of a robot in a closed loop exploration task.

II. Background and Related Work

A wide variety of tactile sensors have been developed over the past 30 or so years [15], and a broad spectrum of novel approaches to transducing tactile information [16]–[18]. Recently, as the capabilities of dexterous robotic manipulators has been improving, there has been increasing demand for integration with robust tactile sensors. These sensors will undoubtedly require the ability to detect a range of tactile features, necessitating multimodal tactile sensing. Presently, few of the available tactile sensors have addressed the requirement for multimodality and typically they cost thousands of dollars.

Manuscript received September 10, 2017; accepted December 26, 2017. Date of publication January 17, 2018; date of current version February 1, 2018. This letter was recommended for publication by Associate Editor J. McInroy and Editor J. Wen upon evaluation of the reviewers comments. The work of N. Pestell was supported by an EPSRC IAA award on a "Tactile smart grasping system." The work of N. F. Lepora was supported in part by a grant from the Engineering and Physical Sciences Research Council (EPSRC) on "Tactile superresolution sensing" (EP/M02993X/1), in part by a Leadership Award from the Leverhulme Trust on "A biomimetic forebrain for robot touch" (RL-2016-39), and in part by an EPSRC IAA award on a "Tactile smart grasping system." *(Corresponding author: Nicholas Pestell.)*

The authors are with the Department of Engineering Mathematics and Bristol Robotics Laboratory, University of Bristol, Bristol RG40 4QR, U.K. (e-mail: np0877@bristol.ac.uk; jl15313@bristol.ac.uk; jonathan.rossiter@bristol.ac.uk; n.lepora@bristol.ac.uk).

This letter has supplementary downloadable material available at http://ieeexplore.ieee.org, provided by the authors. The Supplemental Material contains a video showing a demonstration of the final experiment presented in the submitted manuscript. This material is 8.72 MB in size.

Digital Object Identifier 10.1109/LRA.2018.2794609

In [2] a multimodal tactile skin is presented that comprises of flexible polymer materials and metal thin film resistor MEMS devices. The sensor can measure temperature with a nickel resistance temperature device (RTD), thermal conductivity with a gold heater and nickel RTD pair and hardness using a nickel-chrome alloy strain-gauge.

A bio-inspired tactile sensor is presented in [4]. The sensor comprises of two devices; i) a nine degree of freedom micro-electromechanical (MEMS) providing information about orientation by means of a magnetometer and accelerometer and rate of vibrations with a gyroscope; and ii) a deep MEMS barometer which is used for sensing un-localised pressure and high-frequency pressure changes.

The BioTac [3], [19] is a well known multimodal tactile sensor. It contains an array of impedance electrodes for sensing static spatial properties at a high-resolution, a hydro-acoustic pressure sensor, which can be used for high-frequency features such as texture [20], and a thermistor for sensing temperature [6]. The BioTac integrates three distinct technologies into one fingertip-sized sensor. Whilst this is an impressive achievement, it does increase both complexity and cost, both of which are major factors when considering that a fully equipped tactile humanoid will likely have five tactile sensors on each hand. Indeed, all of the aforementioned multimodal devices suffer from this scaling problem.

As seen with the preceding literature, multimodal tactile sensing is generally applied to sensing with i) high spatial resolution and ii) high-frequency vibrations for textures or slip. A different approach to multimodality is taken in [14]. Here, a dual-mode compliant optical tactile sensor estimates force with two distinct modes: i) a high-resolution 'explore mode,' where image processing is used to infer motion of the sensor skin from a sequence of images from which force is accurately estimated and ii) a high-frequency 'reflex mode' is used for quick reactions and rough estimation of force. A single optical device is used for acquiring images which can return data with high-bandwidth at a cost of resolution or vice versa.

This study presents a sensor which is an evolution of a 3D-printed optical tactile sensor called the TacTip [8], [11]. Originally developed in 2009, it is an optical tactile sensor which draws influence from the structure of the human fingertip. The TacTip works on the principle of transduction from tactile stimulation through a compliant flesh-like structure to an optical signal which is captured via a camera system. An array of pins on the inside of the sensing surface is tracked via an image processing algorithm to reduce dimensionality and the pin deflections are mapped back to a classification of the tactile stimulation [21]. Here we aim to address the need for cheap and simple multimodal sensing by replacing the CCD webcam used in the TacTip with a tracking image sensor similar to that used in [14]. We adopt the core bio-inspired approach to transduction and much of the fabrication methods from a series of publications with the TacTip [9]. We take a completely novel approach to extracting information from the image, where no-image preprocessing is used to reduce dimensionality; raw pixel values from a 30×30 pixel image are used as features for classification of tactile stimulation.

Largely unconsidered in robotics, is the modality of pain. With clear benefits in nature for self-preservation, it is an idea that could transfer naturally to robotics. In mammalian physiology, pain sensing is through mechanoreceptor nerve endings for type II Aδ sensory nerve fibres. These fibres are responsible for mediating temperature, pressure, well-localised 'fast' pain [22], and are known to be involved in both noxious and innocuous tactile sensing below the pain threshold [23]. Here we apply a high-speed modality to predict and modulate contact depth (proportional to pressure) and we draw the analogy between this modality and pain reception in mammals with type II Aδ sensory nerve fibres.

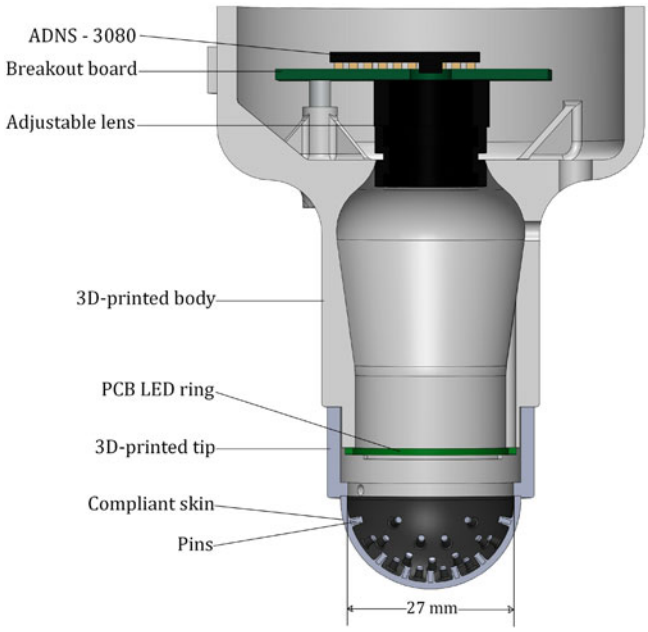

Fig. 1. Computer modelled cross section view of the sensor assembly. The two main components are i) the 3D-printed body, housing the ADNS-3080 image tracking system and the PCB LED ring and ii) the 3D-printed tip with a compliant sensing surface and pins.

III. Materials and Methods

A. Sensor design

1) Hardware: The presented sensor, shown in Fig. 1, is comprised of two main components: a compliant tip and a rigid body, housing the optical sensing element and electronics. The two components interlock via a bayonet fitting.

The tip is 3D-printed and consists of an outer 'skin' (Tango Black+ (Shore A 26-28)) and a rigid bayonet fitting (Vero White). Both elements are printed as a single part. The skin is deformable, enabling transduction of tactile information; it has the added feature of making the sensor compliant which is important when interacting with delicate or unknown objects. The inside surface of the skin (Fig. 2) features a concentric pattern of white dots (Vero White) on the end of short pins (Tango Black+). Once printed, the space between the inside of the skin and an inserted acrylic lens is manually filled with a clear silicone gel (RTV27905, Techsil UK ($\sim$Shore OO 10)). The gel provides stiffness to the tip which helps to minimise hysteresis whilst still enabling compliance. The overall diameter of the tip is $\sim$27 mm which is a $\sim 33\%$ reduction from previous TacTip versions [8], [10].

The sensor body (ABS thermoplastic) is 3D-printed. It is responsible for housing the image tracking system. The

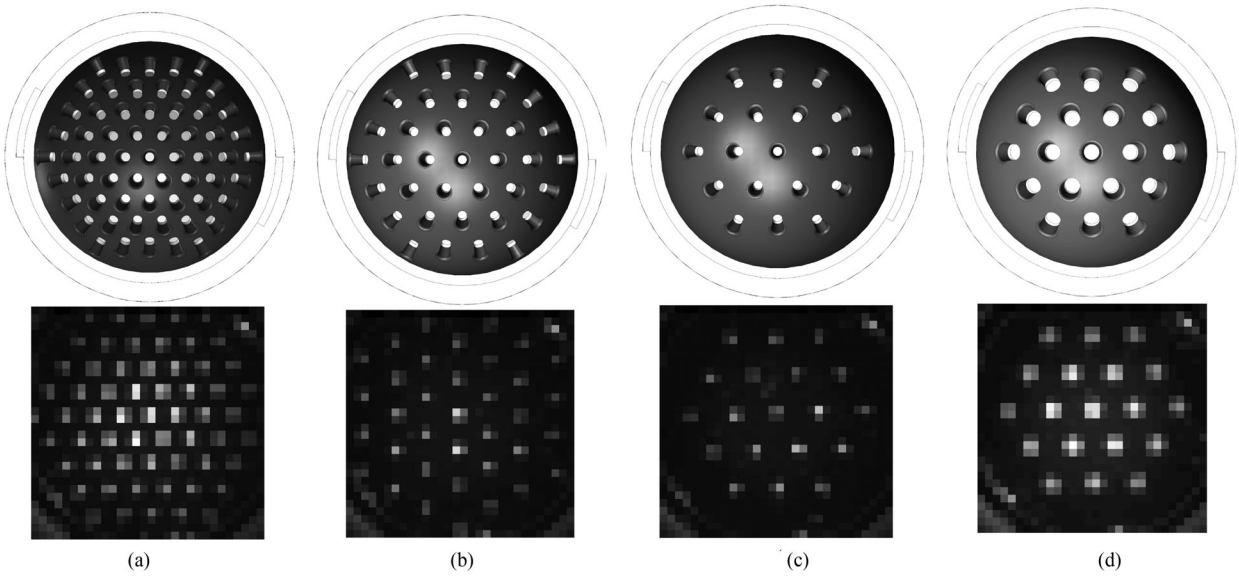

Fig. 2. Computer models of four alternate pin layouts (top row) and respective tip images capture by the ADNS-3080 below. Tip-A features the same pin size and spacing as the latest TacTip version - diameter ∼1 mm, spacing ∼3 mm; Tip-B - diameter ∼1 mm, spacing ∼4 mm; Tip-C - diameter ∼1 mm; spacing ∼4.5 mm; Tip-D - diameter ∼1.7 mm, spacing ∼4.5 mm.

specific focal length and view angle of the image tracking system resulted in the selected shaft length (∼38 mm) and diameter (∼23 mm). It also features a bayonet mount for easy replacement of modular tips and houses a PCB ring of six LEDs for illuminating the inside of the tip.

2) Image Tracking System: The principal novelty of the presented sensor is the optical sensing element. We use a tracking image sensor, *ADNS-3080, Avago Technologies* [7], designed for use in optical computer mice. The sensor uses Complementary Metal-Oxide-Semiconductor (CMOS) technology. It combines an image acquisition system (IAS), acquiring a 30 × 30 pixel image, and a digital signal processor (DSP), which processes the images to generate a series of statistics into a single chip [24]. The frequency of the IAS has a default value of 2000 Hz and is programmable to a maximum value ∼6400 Hz. Importantly, the sensor has two modes of operation: high-speed statistic mode, where a single value is available at the IAS frequency; and frame capture mode, where the sensor sends each pixel value of the 30 × 30 pixel image over the serial interface in sequence, thus forcing a frame rate which is ∼900 times lower than the high-speed statistic mode.

The presented sensor uses an ADNS-3080 on a breakout-board with an adjustable lens attachment (focal length = 4.2 mm, view angle = 86°). The ADNS-3080 is interfaced with an 8-bit, 16 MHz microcontroller, *Arduino Nano* (mounted on the outside of the sensor body), via a 4-wire serial interface (SPI). Data is then passed to an external PC application (Python, pySerial) over an asynchronous serial transmission.

3) Robotic System: For all experiments carried out in the present study we use a six degree-of-freedom robot arm (IRB 120, ABB Robotics) to which our sensor is mounted as an end-effector. The arm can precisely and repeatedly position the sensor (absolute repeatability 0.01 mm). A custom 3D-printed mount is bolted to the rotating (wrist) section of the arm to which the sensor is attached via a bayonet mechanism.

B. High-Speed Sensing

We use the ADNS high-speed mode, to enable the first distinct modality (mode-HS) of the presented tactile sensor. The illuminated dots on the inside of the sensing surface provide visual features which the IAS detects. The DSP generates statistics based on the motion of these features when the sensing surface experiences stimulation. The statistics are; relative x and y movement between sequential images, shutter timings, maximum pixel value and image quality (a measure of the number of features present in the image).

This mode of operation offers extremely high frequency because a single byte of data is used to represent the whole image. We consider mode-HS as having a response which is analogous to that of free nerve endings of type II Aδ sensory nerve fibres in human tactile perception which are rapidly adapting mechanoreceptors responsible for 'fast' pain [22].

C. High Resolution Sensing

In this modality (mode-HR), we make use of the whole 30 × 30 pixel image (see Fig. 2). A higher resolution of tactile sensing, compared with mode-HS, is attainable because of the increased dimensionality. This comes at a cost of bandwidth (∼3 Hz) which is significantly lower than mode-HS.

White dots, located on the tip of each pin, provide optical output for transduction of tactile information, whilst the pins provide amplification of the signal. This is analogous to the interaction between Merkel cells and intermediate ridges within the human fingertip [10], where intermediate ridges help to focus the stress of contact as well as magnifying the signal [25]. The dots move relative to the optical system, due to tactile stimulation, resulting in pixel change. The raw values of all 900 pixels (6-bit resolution) are used as features for tactile perception. This is a completely novel approach compared to past work with the TacTip, where pin deflections were used.

D. Alternate Pin Layouts

The pin layout used with TacTip in recent work has proven effective [12], however, in this study we apply a novel approach of using the raw pixel values instead of pin positions and hence consider that this may not be the best arrangement of pins. For example, drastically differing stimulation could result in the same value for a pixel if different pins are imaged by the same point on the CMOS array. We therefore hypothesise that a less dense pin layout will result in fewer pin overlaps and thus better tactile perception.

Four alternate pin layouts are considered, shown in Fig. 2. Tip-A features a pin spacing of $\sim$3 mm and pin diameter of $\sim$1 mm, these dimensions were chosen to match the latest TacTip version. Tip-B and Tip-C have the same pin diameter as the latest TacTip version but with increased pin spacing of $\sim$4 and $\sim$4.5 mm respectively. Finally, Tip-D has a pin spacing of $\sim$4.5 mm but with an enlarged pin diameter of $\sim$1.7 mm.

E. Task: Contact Depth Control

Here we consider the task of controlling the contact depth, z: we require the robot to follow a target trajectory where position is modulated by measurements from the high-speed mode of the tactile sensor.

1) Data Collection and Calibration: For the four alternate pin layouts shown in Fig. 2, image statistics were collected for 5 second intervals at constant compressions on a flat stimulus. $N_z = 20$ depths were used spanning -5 mm $\leq z_i \leq 0$ mm. Measurements are taken relative to the where the sensor tip makes initial contact with the stimulus. An average value at each step is then used to fit a Gaussian process regression (MATLAB, fitrgp) which is used as calibration in the depth control task.

2) Testing: To test the depth control, a task was created where the robot is required to follow a sinusoidal target trajectory in z whilst remaining in constant contact with the flat stimulus used for calibration. The control is a closed-loop system using only tactile feedback from mode-HS to modulate the z-position of the sensor.

Before each step move in z, one sample from the high-speed mode is taken, after which we estimate the depth according to the calibration curve. The robot then modulates its z-position using a control policy, π, by performing a relative move from the current perceived depth towards a target, which is defined by sinusoidal trajectory in z,

$$\Delta z_i = \pi_i[z_{\mathrm{dec}}] = (z_{\mathrm{target},i} - z_{\mathrm{dec}}), \tag{1}$$

z_{dec} is the perceived depth and $z_{\mathrm{target,i}}$ is the target at step i. Here we use just one sample for predicting the depth in order to minimise the reaction time and benefit from the high sampling rate provided by mode-HS.

F. Task: Perception

For high-resolution sensing, using mode-HR, we implement a biomimetic perception algorithm previously shown to achieve superresolved acuity with the TacTip [11]. These methods have successfully been applied to a contour following task [13], and here we re-implement the same methods, applied to a different sensor and a different representation of the data (pixel values instead of pin deflections).

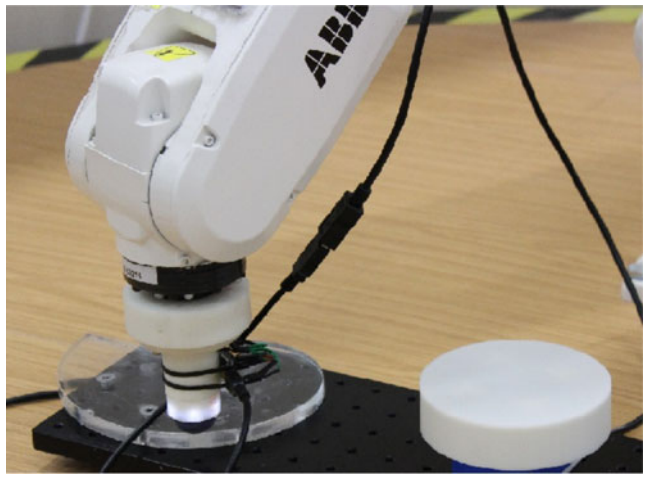

Fig. 3. Sensor mounted as an end-effector on the robot arm used for experiments. The two stimuli used are also shown: circle (right) and non-uniform volute (left).

1) Data Collection: For each of the four alternate pin layouts show in Fig. 2 we collect two distinct datasets; the first is used for training and the second for testing through off-line validation. The robot makes successive taps onto the stimulus edge and records 5 frames with the sensor held statically at the bottom of the tap ($\sim$2 mm of compression of sensing surface). Over the 5 frames, pixel values for all $N_{\mathrm{dims}} = 900$ are recorded yielding a total of 4500 sensor values. The stimulus used was a 3D-printed circular object (diameter $=$ 107 mm) with a 90° edge, shown in Fig. 3.

For each dataset, taps are performed at a discrete set of angles and radial positions relative to the stimulus edge (the same for both sets). We use $N_\theta = 9$ angles spanning $-40^\circ \leq \theta_i \leq 40^\circ$ and $N_r = 21$ radial positions spanning -10 mm $\leq r_l \leq 10$ mm centred on the edge of the stimulus, yielding a total of $N_{\theta,r} = 189$ positions per dataset.

2) Decision Making: We adopt a standard 'histogram' likelihood model [12]. The data, d, is considered as a time series of sensor values,

$$d = \{s_k(j) : 1 \leq j \leq N_{\mathrm{samples}}, 1 \leq k \leq N_{\mathrm{dims}}\}, \tag{2}$$

j denotes the time sample and k denotes the sensor dimension (pixels). After each test tap, $N_{\theta,r}$ likelihoods are calculated, one for each position, using a measurement model of the training data.

$$\log P(d|r_l, \theta_i) = \sum_{k=1}^{N_{\mathrm{dims}}} \sum_{j=1}^{N_{\mathrm{samples}}} \frac{\log P_k(s_k(j)|r_l, \theta_i)}{N_{\mathrm{samples}} N_{\mathrm{dims}}}, \tag{3}$$

where θ_n and r_l are competing angle and radial position hypothesis respectively. The probabilities, $P_k(s_k(j)|r_l, \theta_i)$ are found with a histogram method applied to training data for each class. The samples, s_k, are binned into $N_{\mathrm{bins}} = 100$ equal intervals. This is transformed to a probability distribution by normalising over the total number of samples at each class.

$$P_k(s_k|r_l, \theta_i) = P_k(b|r_l, \theta_i) = \frac{n_{kli}(b) + \epsilon}{\sum_{b=1}^{N_{\mathrm{bins}}} n_{kli}(b)}, \tag{4}$$

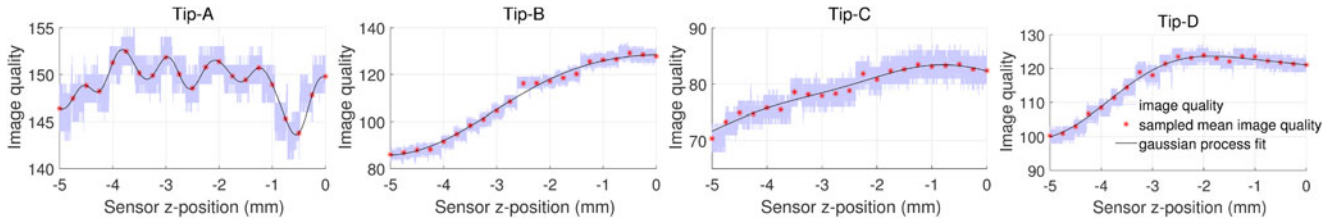

Fig. 4. Image quality statistic plotted against depth of compression on a flat stimulus for the four pin layouts shown in Fig. 2. The raw data (shown in grey) was recorded at constant depths with a 0.25 mm separation for 5 seconds at each depth. The red markers show the mean value at each depth and the line is a Gaussian regression fit.

where $n(b)$ is the total number of sample counts in bin b. Using a constant offset, $\epsilon << 1$, avoids taking the log of zero.

A decision regarding the sensor state is made each time new sensory data becomes available. The decision is made according to a maximum-likelihood criterion.

$$\theta_{\text{dec}} = \arg\max_{\theta_i} P(d|\theta_i) = \arg\max_{\theta_i} \sum_{l=1}^{N_r} P(d|\theta_n, r_l), \quad (5)$$

$$r_{\text{dec}} = \arg\max_{r_l} P(d|r_l) = \arg\max_{r_l} \sum_{i=1}^{N_\theta} P(d|\theta_i, r_l). \quad (6)$$

Likelihoods, $P(d|\theta_i)$ and $P(d|r_l)$, are found by marginalising the joint likelihood over radial position and angle respectively.

To test the perception, we perform off-line validation, computing average angle and radial errors, e_θ, e_r, with 10,000 samples randomly selected from the test set.

G. Task: Contour Following

In the presented exploration task, the robot is required to follow the edge of an unknown object using only tactile feedback. Tactile contour following requires both sensitive and robust perception. It is therefore an ideal task to measure the performance of the high resolution sensing modality.

1) Data Collection and Training: For training the robot we use the same training dataset as in Section III-F1. The procedure for building the likelihood model is also the same.

2) Testing: We implement a 'tactile servoing' approach for robot control throughout the contour following task which was initially implemented with the TacTip [13]. Here we outline the approach, for a detailed description of the methods, we refer the reader to the original text [13].

The robot is controlled through a perception-action cycle. The sensor is tapped onto the stimulus edge where 5 frames are recorded. The sensor angle and radial position, relative to the stimulus edge, are then perceived according to the procedure described in Section III-F2. This perception informs the actions to select via a deterministic control policy.

The method for controlling the robot involves an action selection policy, where the sensor attempts to maintain an optimal position for perception. For the purpose of tactile contour following, action selection defines two procedures: i) tactile servoing, which attempts to maintain a constant angle, θ_{fix}, relative to the stimulus edge based on the perceived edge angle θ_{dec} and ii) radial repositioning, where the sensor relocates perpendicularly to the perceived edge towards a pre-set fixation radial displacement, r_{fix}. The two policies are described by the following two equations respectively:

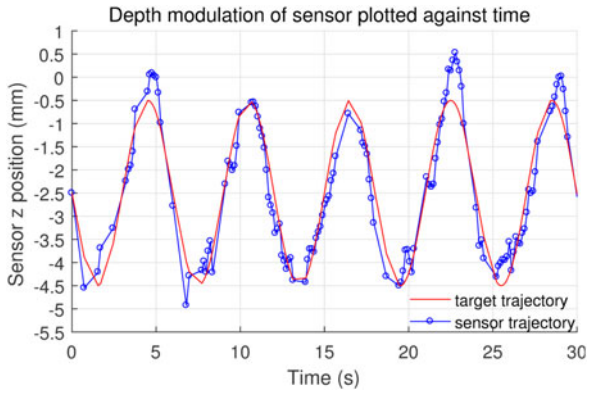

Fig. 5. Sensor trajectory in z (blue) and target (red) vs. time. Blue markers show the sensor position at each step.

$$\Delta\theta = \pi_\theta[P(d|r_l, \theta_n)] = [g_\theta(\theta_{\text{fix}} - \theta_{\text{dec}})]_i, \quad (7)$$

$$\Delta r = \pi_r[P(d|r_l, r_l)] = [g_r(r_{\text{fix}} - r_{\text{dec}})]_l, \quad (8)$$

where g_θ and g_r are the angular and radial gain factors respectively (set to 0.5 or 1 in previous work [13]) and $[.]_l$ and $[.]_i$ shows that the action is rounded down to the nearest class. Here the fixation points are chosen as the centre of the perceptual ranges, $\theta_{\text{fix}} = 0$ and $r_{\text{fix}} = 0$.

Supplementary to action selection is an exploration policy. Also defined by perception, the robot moves the sensor in a direction tangential to the perceived edge angle by a fixed amount, $\Delta e = 3$ mm, and therefore follows the contour.

IV. Results

A. Contact Depth Control

Of the five statistics, only image quality provided a useful response. All other measures were unresponsive when exposed to tactile contact which is consistent with observations made previously [14]. Fig. 4 shows the image quality (grey) plotted against contact depth for the four considered pin layouts. Also displayed is the average value for image quality at each step (red markers) and a Gaussian process regression (black line), fitted to the average values.

The sensor exhibits no noticeable relationship between image quality and contact depth with Tip-A. Tips B-D exhibit a general relationship of decreasing image quality with increasing contact depth. We note that only Tip-B shows a monotonic relationship

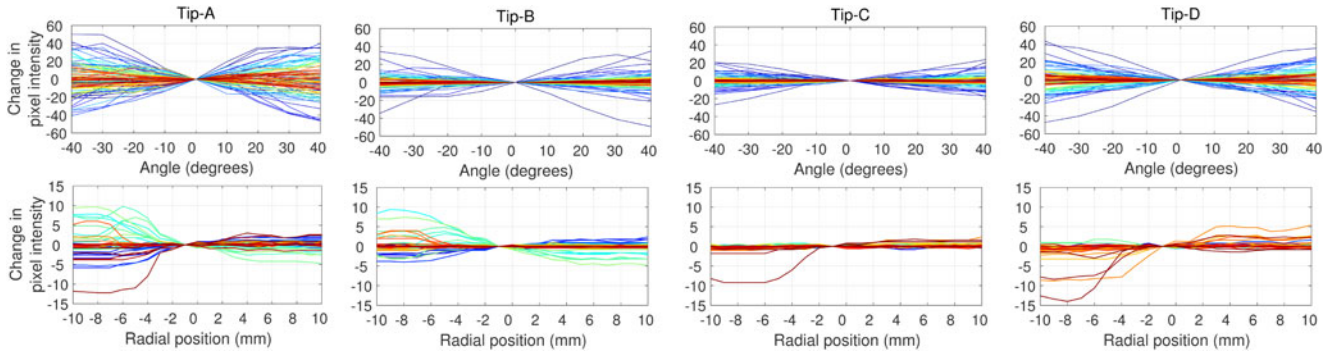

Fig. 6. Change in pixel intensity for 100 selected pixels, plotted in different colours, against angle (top) and radial distance (bottom) for the four pin layouts shown in Fig. 2. The values are plotted as relative to the values at class zero for both angle and radius, ($\theta = 0$, $r = 0$), above and below respectively. The pixels are selected for each plot to display maximum variance.

over the full range. Furthermore, the range of sensor output is significantly higher for Tip-B ($\sim$43) than Tip-C ($\sim$13) or D ($\sim$24). Hence, we conclude that the best pin layout for depth control, when using image quality, is given by Tip-B.

To test the performance of our depth control method we tasked the robot with following a predefined z-trajectory (see Section III-E2). We use Tip-B for this test since it was found to have the best relationship between image quality and depth (Fig. 4). Results are shown in Fig. 5.

The sensor successfully follows the target to within $\sim$1.1 mm and a mean absolute discrepancy of 0.37 mm. Divergence from the target is mainly observed at the maximum z-position which may be explained by hysteresis: magnified by a fast step rate, the compliant tip requires time to equilibrate after each step. Also, sensor noise (see Fig. 4) may have a negative impact on accuracy of the prediction. The effect of noise would be reduced by using the mean of multiple samples at each step, however, this reduces the speed of prediction.

It is worth noting that the step rate here is defined, not only by the sensor bandwidth but, more directly, by latency in the robot control system: a finite amount of time is required for the client to send control commands over a network to the robot server and for the robot to execute that command. We therefore stress that the use of mode-HS minimises the response time and a lower bandwidth device would reduce the step rate.

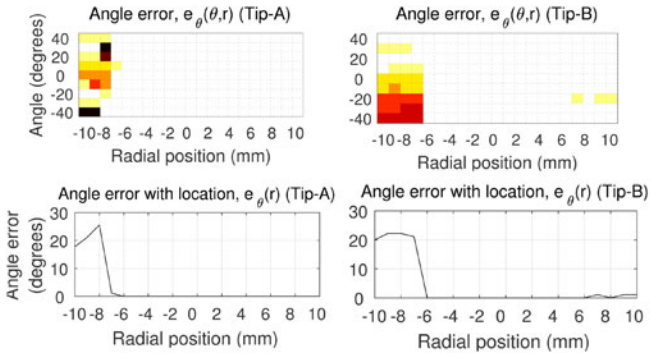

Fig. 7. Angular perception errors, with angle and radial position, $e_\theta(\theta, r)$ (top) and with radial position, $e_\theta(r)$ (bottom) for tips A and B. Above errors are a heat map: 70° (black) - 0° (white).

TABLE I
MEAN ANGLE AND RADIAL ERRORS IN AN OFF-LINE PERCEPTION TASK

	Mean angle error, e_θ (degrees)	Mean radial error, e_θ (mm)
Tip-A	0	0.06
Tip-B	1.4	0.07
Tip-C	0.4	0.01
Tip-D	1.5	0.06

Values were computed ignoring the radial position classes $-10 \leq r \leq -8$.

B. Location and Angle Perception

Data collected with mode-HR through the procedure described in Section III-F1 for the four tips are shown in Fig. 6. Here we show the change in pixel intensity, relative to values at $\theta = 0°$ and $r = 0$ mm above and below respectively, for 100 selected pixels, shown in different colours (pixels selected to display maximum variance). The plots show significant variation in pixel values across the sample range, suggesting that pixels are sufficient for tactile perception. Tip-A appears to exhibit the most variation whilst Tip-C exhibits the least.

We computed error values as absolute discrepancies in perceived angle and radius with the ground truth, averaged over multiple test runs, as a function of angle and radial position; $e_\theta(\theta, r) = \langle \mid \theta_{\text{dec}} - \theta \mid \rangle$ and as a function of radial position; $e_\theta(r) = \sum_{i=1}^{N_\theta} e_\theta(r, \theta_i)/N_\theta$. All four tips achieved good perceptual accuracy using the perception method described in Section III-F2. These error values are shown for tips A and B in Fig. 7. We note that there is near perfect angle perception at positions $r \geq -8$ mm. Below -8 mm the sensor taps are in free space, hence perceptual performance here is poor. Tip-B experiences some loss of perceptual accuracy as contact is further onto the stimulus, as expected because less of the edge is felt by the sensor. All average angular and radial errors were below 2° and 0.1 mm respectively. The values for all four pin layouts are shown in Table I.

C. Contour Following

The perception is tested in a general contour following task to examine the robustness to previously unseen stimulation. According the procedure described in Section III-G2, the robot is required to follow the contour edge of a circular object (diameter 110 mm) using the same training dataset as used in

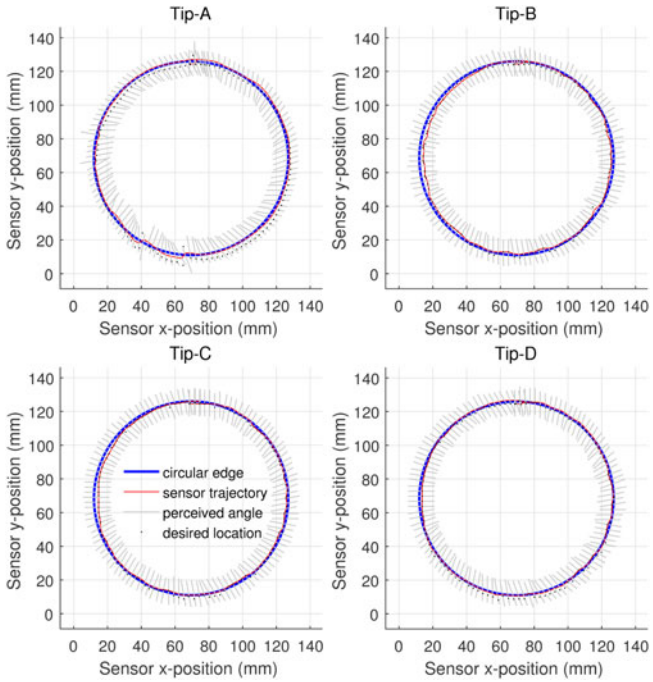

Fig. 8. Trajectories for a contour following task around a circle (diameter 110 mm) (blue curve) for four pin layouts. Radial and angular gains are 0.5.

TABLE II
MEAN ANGLE AND RADIAL ERRORS FOR THE FOUR ALTERNATE PIN LAYOUTS IN A CONTOUR FOLLOWING TASK

	Mean angle error, e_θ (degrees)	Mean radial error, e_θ (mm)
Tip-A	14.3	3.40
Tip-B	7.6	2.56
Tip-C	5.1	2.57
Tip-D	7.8	2.29

Section IV-B. A radial fixation point centred on the range, $r_{\text{fix}} = 0$ was chosen. This location is validated by the results from the perception task (Section IV-B). We performed the task with all four tips and the results are shown in Fig. 8.

Good performance was found with radial and angular gains $g_r, g_\theta = 0.5$ and exploration steps $e = 3$ mm. All four tips successfully completed the task. Visual inspection of the trajectories shows minimal variation in performance: the worst performing was Tip-A whilst the best performing was Tip-D. Absolute errors in angular and radial perception are shown in Table II. The perceptual accuracies appear to confirm the performance in contour following. Interestingly, this result counters the angular perception results from Section IV-B, suggesting that, whilst Tip-B may under-perform when perceiving angles that have previously been observed, the perception with this tip may generalise better than Tip-A to perceive stimulation that is dissimilar to the training set.

D. Combined Modality Control

To demonstrate the benefits gained from dual-modality we design a task where the robot uses both modes. Using Tip-B, the robot must follow the edge of a previously unseen stimulus, trained only with the circle shape used for previous experiments. A non-uniform volute shape (see Fig. 3) is used, where the radius of curvature varies from 20 mm to 50 mm.

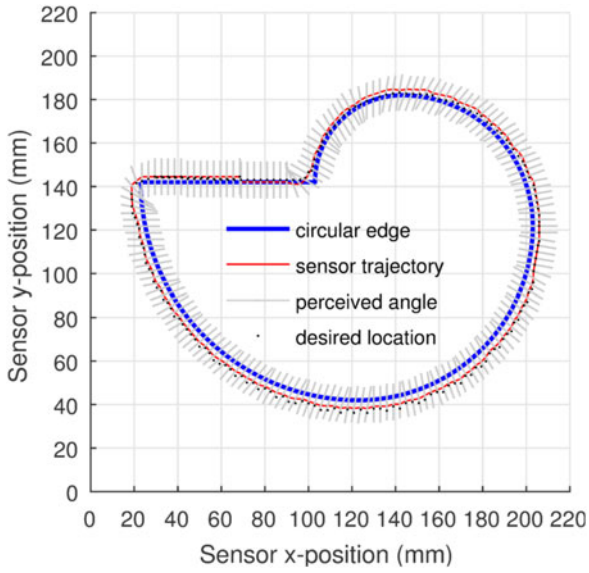

Fig. 9. Trajectory for contour following task on a non-uniform volute (blue curve). Radial and angular gains are set to 0.5.

The exact height of the volute is unknown to the robot, as well as the location of the edge. To successfully apply the training data to the unseen object, the sensor must attain the same relative height. This is achieved with the use of mode-HS. First, the robot moves the sensor down to a rough approximation of centre of the test object. The image quality measure is monitored and initial contact is detected by applying a threshold criterion. After contact is detected, the sensor height is modulated to the correct depth according to (1). The robot then locates the edge of test object by monitoring image quality whilst moving in the x, y-plane. The edge is detected when image quality rises above a threshold.

Once the edge is detected, the robot follows the contour according to the procedure used in earlier tasks. Results of contour following on the volute, with an automated dual-mode approach to depth and edge location, are shown in Fig. 9.

The robot successfully detects initial contact and locates the edge of the volute using mode-HS. The robot then correctly follows the contour, suggesting that the depth is modulated accurately and general training data can be applied to the methods in order to follow the contour of an unknown, non-uniform shape using the second modality.

V. DISCUSSION

In this study, we presented a novel, dual-modal, optical tactile sensor, without image processing or a high-resolution imaging system. The sensor was tested in a series of tasks, aimed at assessing its ability to use a high-speed modality for depth modulation and a second, high-resolution modality for perceiving angle and radial position relative to an edge. We examined the robustness of the high-resolution perception in a tactile contour following task, using the methods developed in [13]. Finally,

we presented a task requiring both modalities, where the robot follows the contour of a previously unseen object, where the exact object location and depth was unknown.

The sensor achieved good accuracy in both the depth control and angle and radial position perception tasks. The high-resolution sensing was robust enough for successful contour following around the circle and this generalised to the non-uniform shape after using the high-speed modality to find the object's height and locate the edge.

We compared the performance of four alternate pin layouts in the depth control, perception and contour following tasks. Interestingly, there was little variation in performance between the four pin layouts within the high-resolution mode when perceiving angle and radial position. This was a surprising result; however, our study was limited to concentric patterns of pins which, whilst necessary for the TacTip, could be replaced by an arbitrary pattern in the case where raw pixel values are used as features. Hence, further study may elicit a more optimal pin design. The pin layout had a large influence on the high-speed sensing modality: Tip-B showed the most sensitivity in the image quality statistic to tactile stimulation. Image quality is a measure of the number of features present in the frame [7]. It appears to be maximised when pins are at the optimum distance from the lens and reduces as the pins move out of focus. We suggest that Tip-B has the best balance between pin spacing, number of pins and pin size for the image quality algorithm to detect each pin as a separate feature. The ADNS-3080 may struggle to separate the pins of Tip-A, for example, as separate features, whilst tips C and D have fewer pins, yielding a lower overall value in image quality.

Furthermore, the technology used in the presented sensor has enabled dual-modality on a single integrated chip making it a cost effective and compact option for future progression in tactile sensing. Here we focus on using the high-speed mode as a depth control sensor which is necessary to achieve robust tactile sensing in unknown environments. We also stress the importance of a high-speed modality in modulating contact depth (related to pressure) in minimising the risk of sensor damage. Pain reception, in nature, provides a rapid response to stimulation when compared to more sensitive or higher resolution tactile modalities. Indeed, the response to pain is often a reflex, where the stimulation signal bypasses the brain and directly excites motor control, demonstrating that a rapid response to compromising environments is necessary.

The presented sensor is an encouraging progression for optical tactile sensing. Importantly, this study demonstrated that image processing is unnecessary for optical tactile sensors and accurate and robust perception is attainable with very low-resolution images when using raw pixel values as features. This has implications for future technologies such as reducing cost and miniaturisation.

ACKNOWLEDGMENT

We thank research group members; B. Ward-Cherrier, L. Cramphorn, K. Aquilina, S. Baker, and J. James, for help with experimentation. The data used in this letter are available for download at 10.5523/bris.1s5pofgyr9i9v1ypc1zhdh8b8b.

REFERENCES

[1] R. L. Klatzky and S. J. Lederman, "Toward a computational model of constraint-driven exploration and haptic object identification," *Perception*, vol. 22, no. 5, pp. 597–621, 1993.

[2] J. Engel, J. Chen, Z. Fan, and C. Liu, "Polymer micromachined multimodal tactile sensors," *Sensors Actuators A, Phys.*, vol. 117, no. 1, pp. 50–61, 2005.

[3] N. Wettels, J. A. Fishel, and G. E. Loeb, "Multimodal tactile sensor," in *The Human Hand as an Inspiration for Robot Hand Development*. Berlin, Germany: Springer, 2014, pp. 405–429.

[4] A. C. Alves de Oliveira and E. Petriu, "Multimodal bio-inspired tactile sensing module for surface characterization," *Sensors*, vol. 17, no. 6, 2017, Art. no. 1187.

[5] P. Mittendorfer and G. Cheng, "Humanoid multimodal tactile-sensing modules," *IEEE Trans. Robot.*, vol. 27, pp. 401–410, Jun. 2011.

[6] D. Xu, G. Loeb, and J. Fishel, "Tactile identification of objects using bayesian exploration," in *Proc. IEEE Int. Conf. Robot. Autom.*, 2013, pp. 3056–3061.

[7] Avago Technologies, "ADNS-3080 High-Performance Optical Mouse Sensor," datasheet, 2009.

[8] C. Chorley, C. Melhuish, T. Pipe, and J. Rossiter, "Development of a tactile sensor based on biologically inspired edge encoding," in *Proc. 2009 Int. Conf. Adv. Robot.*, 2009, pp. 1–6.

[9] B. Ward-Cherrier, N. Pestell, L. Cramphorn, B. Winstone, M. E. Giannaccini, J. Rossiter, and N. F. Lepora, "The TacTip Family: Soft Optical Tactile Sensors with 3D-Printed Biomimetic Morphologies," *Soft Robot.*, Jan. 2018.

[10] L. Cramphorn, B. Ward-Cherrier, and N. F. Lepora, "Addition of a biomimetic fingerprint on an artificial fingertip enhances tactile spatial acuity," *IEEE Robot. Autom. Lett.*, vol. 2, no. 3, pp. 1336–1343, Jul. 2017.

[11] N. F. Lepora and B. Ward-Cherrier, "Superresolution with an optical tactile sensor," in *Proc. 2015 IEEE/RSJ Int. Conf. Intell. Robots Syst.*, 2015, pp. 2686–2691.

[12] N. F. Lepora, "Biomimetic active touch with fingertips and whiskers," *IEEE Trans. Haptics*, vol. 9, no. 2, pp. 170–183, Apr.–Jun. 2016.

[13] N. F. Lepora, K. Aquilina, and L. Cramphorn, "Exploratory tactile servoing with active touch," *IEEE Robot. Autom. Lett.*, vol. 2, no. 2, pp. 1156–1163, Apr. 2017.

[14] E. Knoop and J. Rossiter, "Dual-mode compliant optical tactile sensor," in *Proc. 2013 IEEE Int. Conf. Robot. Autom.*, 2013, pp. 1006–1011.

[15] M. R. Cutkosky and W. Provancher, *Force and Tactile Sensing*. Berlin, Germany: Springer International Publishing, 2016, pp. 717–736.

[16] Z. Kappassov, J.-A. Corrales, and V. Perdereau, "Tactile sensing in dexterous robot hands review," *Robot. Auton. Syst.*, vol. 74, no. Part A, pp. 195–220, 2015.

[17] M. Evans, C. W. Fox, M. J. Pearson, N. F. Lepora, and T. J. Prescott, "Whisker-object contact speed affects radial distance estimation," in *Proc. 2010 IEEE Int. Conf. Robot. Biomimetics*, 2010, pp. 720–725.

[18] J. Back, P. Dasgupta, L. Seneviratne, K. Althoefer, and H. Liu, "Feasibility study—Novel optical soft tactile array sensing for minimally invasive surgery," in *Proc. 2015 IEEE Int. Conf. Robot. Systems*, Chicago, Sep. 2015, pp. 1528–1533.

[19] N. Wettels, D. Popovic, V. J. Santos, R. S. Johansson, and G. E. Loeb, "Biomimetic tactile sensor for control of grip," in *Proc. IEEE 10th Int. Conf. Rehabil. Robot.*, 2007, pp. 923–32.

[20] B. P. Delhaye, E. W. Schluter, and S. J. Bensmaia, "Robo-psychophysics: Extracting behaviorally relevant features from the output of sensors on a prosthetic finger," *IEEE Trans. Haptics*, vol. 9, no. 4, pp. 499–507, Oct. 2016.

[21] B. Ward-Cherrier, N. Rojas, and N. F. Lepora, "Model-free precise in-hand manipulation with a 3d-printed tactile gripper," *IEEE Robot. Autom. Lett.*, vol. 2, no. 4, pp. 2056–2063, Oct. 2017.

[22] A. I. Basbaum, D. M. Bautista, G. Scherrer, and D. Julius, "Cellular and molecular mechanisms of pain," *Cell*, vol. 139, pp. 267–84, 2009.

[23] V. Abraira and D. Ginty, "The sensory neurons of touch," *Neuron*, vol. 79, no. 4, pp. 618–639, 2013.

[24] D. Font, M. Tresanchez, T. Pallej, M. Teixid, and J. Palacn, "Characterization of a low-cost optical flow sensor when using an external laser as a direct illumination source," *Sensors*, vol. 11, pp. 11856–11870, 2011.

[25] G. J. Gerling and G. W. Thomas, "The effect of fingertip microstructures on tactile edge perception," in *Proc. First Joint Eurohaptics Conf. Symp. Haptic Interfaces Virtual Environment Teleoperator Syst. World Haptics Conf.*, 2005, pp. 63–72.